Z. Kristallogr. Suppl. **26** (2007) 67-72

Method for quick estimation of the Sb^{3+}/Sb^{5+} content ratio in ATO

B. Gržeta[1,*], E. Tkalčec[2], C. Goebbert[3], M. Takeda[4] and M. Takahashi[4]

[1]Ruđer Bošković Institute, P.O. Box 180, HR-10002 Zagreb, Croatia
[2]Faculty of Chemical Engineering and Technology, University of Zagreb, Marulićev trg 20, HR-10000 Zagreb, Croatia
[3]ItN Nanovation, D-38820 Halberstadt, Germany
[4]Faculty of Science, Toho University, Funabashi, Chiba 274-8510, Japan
[*] Contact author; e-mail: grzeta@irb.hr

Keywords: Antimony tin oxide (ATO), X-Ray powder diffraction, Mössbauer spectroscopy, Sb^{3+}/Sb^{5+} content ratio in ATO

Abstract. A method for estimation of the Sb^{3+}/Sb^{5+} content ratio in antimony-doped tin oxide (ATO) is described. It involves measuring of XRD pattern of ATO sample in a narrow 2θ range and individual profile fitting of diffraction lines 110 and 101. The ratio of full-widths at half-maximum (FWHM) of the lines 110 and 101, $FWHM_{110}/FWHM_{101}$, is correlated with the Sb^{3+}/Sb^{5+} content ratio in the ATO samples. The method resulted from XRD and ^{121}Sb-Mössbauer spectroscopy investigation of ATO samples.

Introduction

Tin oxide, SnO_2, is a wide-band gap semiconductor with transmittance cut-off at 333 nm [1]. It has a tetragonal TiO_2 (rutile)-type structure, in the space group $P4_2/mnm$ [2]. When doped with F, Sb or Mo it becomes a conductor [3,4]. Sb-doped SnO_2 is well known by the name ATO (antimony tin oxide). Thin ATO films possess an excellent combination of superior optical and electrical properties: high transparency in the visible range and high electrical conductivity, which makes them applicable for various optoelectronic devices [3]. However, it was evidenced that the conductivity was not linearly dependent on the Sb-doping level, it increased for lightly-doped SnO_2 and decreased for heavily-doped SnO_2 [5]. Terrier et al. [6] examined the actual doping level of Sb in the doped SnO_2 films, and also the oxidation state of incorporated antimony, by means of X-ray photoelectron spectroscopy (XPS) and secondary ion mass spectroscopy (SIMS). They found that in doping the Sb^{3+} overcame Sb^{5+} content, but they could not ascertain the exact content of antimony for which that occurred. Many structural studies of ATO have been performed so far with the purpose of elucidating the above phenomena [7-10]. The present paper reports a study of the influence of Sb^{3+}/Sb^{5+} content ratio on structural properties of powder ATO samples.

Experimental

The powder SnO_2 sample (sample S0) and ATO samples containing 3.1, 6.2, 11.9 and 14 at% Sb (samples S1-S4) were prepared by a sol-gel technique followed by hydrothermal treatment at 250 °C and 2.5 MPa. The sample S2 was additionally heat treated at 350, 450 and 550 °C for 1 h, then slowly cooled to RT. The antimony content in the samples was determined by both the atomic emission spectroscopy, using a Jobin Yvon JY24 spectrometer, and particle induced X-ray emission (PIXE), using a 3 MeV proton beam. The results of both methods agreed within the experimental error.

The samples were characterized by X-ray diffraction (XRD) using a Philips MPD 1880 counter diffractometer with monochromatized Cu Kα radiation. Unit-cell parameters were determined by taking silicon powder as an internal standard. Calculations were done by means of the computer program UNITCELL [11]. Then, the unit-cell parameters were refined by the whole-powder-pattern fitting method using the program WPPF [12]. The ATO samples were also examined by Mössbauer spectroscopy. The ^{121}Sb-Mössbauer spectra were recorded at 12 K by a Wissel Mössbauer spectrometer system using a $Ca^{121m}SnO_3$ source (16 MBq). Analysis of spectra was performed by a transmission integral method [13].

Results and discussion

X-ray powder patterns indicated that all examined samples were tetragonal, space group $P4_2/mnm$, and isostructural with TiO_2 (rutile). Only sample S4 contained an impurity phase, namely 5 wt% Sb_2O_3. The results of the whole powder pattern fitting for samples S0 and S2 are displayed in figure 1, while the changes of unit-cell parameters with antimony content are shown in figure 2. Both *a* and *c* parameters for the samples S1, S2 and S3 increased with Sb-doping level, while for S4 decreased to the values which could be situated between those for S0 and S1. Such behaviour of the cell parameters indicated a possibility that both Sb^{3+}

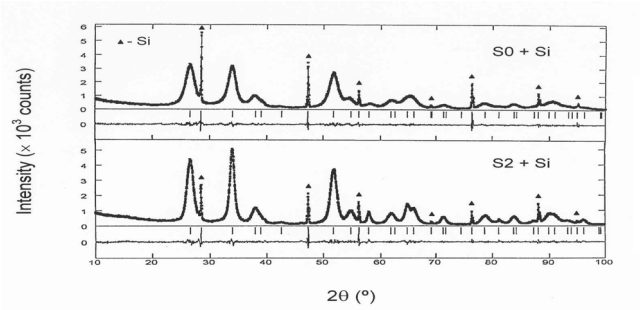

Figure 1. Whole-powder-pattern fitting results for the samples S0 (R_{wp}=0.063) and S2(R_{wp}=0.065).

and Sb^{5+} ions were substituted for Sn^{4+}, but with variable Sb^{3+}/Sb^{5+} content ratio. Unit-cell parameters of the annealed sample S2 decreased with the increase in thermal treatment temperature as seen in figure 3. This suggested that oxidation of the antimony ion Sb^{3+} took place on annealing. As seen in figure 1, diffraction lines were broadened indicating the nanosized crystallites in the samples. The line broadening was anisotropic. The line 110 was the broadest, while the line 101 was the narrowest one for all the samples. Both the line

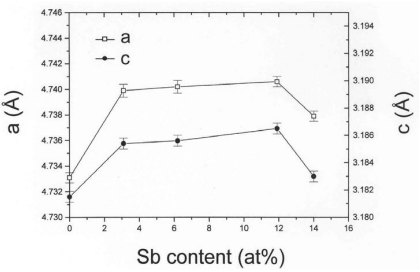

Figure 2. Unit-cell parameters of the samples S0-S4.

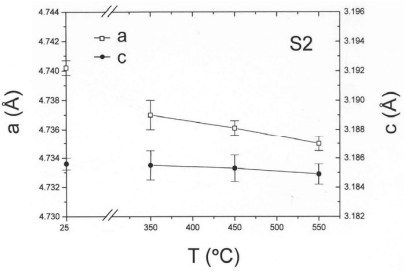

Figure 3. Unit-cell parameters of the annealed sample S2.

broadening and line anisotropy were dependent on the Sb doping level, and also on annealing temperature (examined for the sample S2), as shown in figure 4. For the as-prepared samples (figure 4 (A)), the lines of S0 showed the greatest broadening. Incorporation of Sb up to 11.9 at% decreased the line broadening and increased the line anisotropy. For S4 the broadening was bigger again, while the line anisotropy decreased. The XRD patterns of annealed sample S2 (figure 4 (B)) showed that the line broadening increased up to 350 °C, then decreased upon heating at higher temperatures, while the line anisotropy decreased over the whole temperature range.

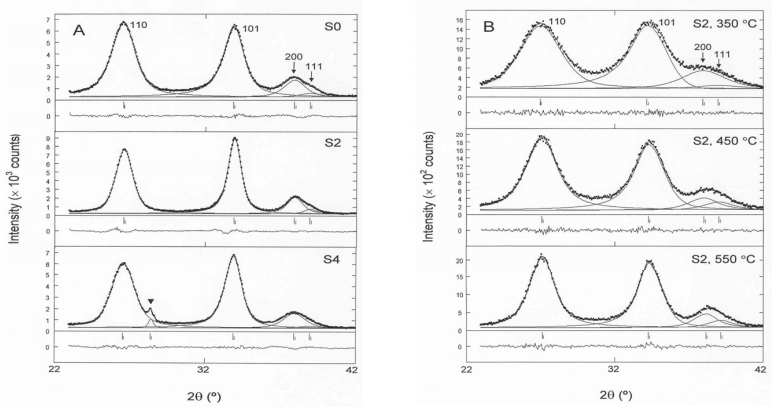

Figure 4. Characteristic part of the XRD patterns: (A) for the samples S0, S2 and S4; (B) for the annealed sample S2. The figures are results of individual profile fitting by the PROFIT program [12]. Black triangle denotes an impurity, Sb_2O_3, in S4.

The crystallite sizes for the samples were determined from the diffraction lines 110 and 101 by the Scherrer formula [14]. The obtained values are listed in table 1. The profiles of 110 and 101 lines were corrected for the instrumental broadening using the nearest profiles of LaB_6 standard, 110 and 111 respectively, and the Ruland relation among the integral line widths for the Cauchy profile [15]. The correction of the observed widths for the broadening

due to the angular separation of the components $K\alpha_1$ and $K\alpha_2$ was done according to Popović [16].

Table 1. Full-widths at half-maximum (FWHM) for the lines 110 and 101 of ATO samples and crystallite sizes in the direction normal to the planes (110) and (101).

ATO sample	Sb content (at%)	T (°C)	FWHM (° 2θ) by PROFIT		FWHM (° 2θ) by WPPF		$D_{\perp(110)}$ (nm)	$D_{\perp(101)}$ (nm)
			110	101	110	101		
S1	3.1(4)	20	1.449(7)	1.107(7)	1.409(6)	1.107(7)	6(2)	8(2)
S2	6.2(6)	20	1.409(6)	0.936(6)	1.356(6)	0.918(6)	6(2)	9(3)
S3	11.9(5)	20	1.356(6)	0.813(6)	1.321(7)	0.836(7)	6(2)	11(3)
S4	14.0(7)*	20	1.838(8)	1.260(8)	1.838(8)	1.274(7)	4(1)	7(2)
S2	6.2(6)	350	3.22(3)	2.96(3)	3.16(3)	2.95(4)	2(1)	2(1)
		450	2.48(2)	2.38(2)	2.43(3)	2.35(3)	3(1)	3(1)
		550	1.94(1)	1.92(2)	1.90(2)	1.88(2)	4(1)	4(1)

* The total content of antimony found in S4 was 19.4(7) at%. A part of it (5.4 at% Sb) crystallized as Sb_2O_3 (namely 5 wt% Sb_2O_3), as found by XRD.

The ^{121}Sb-Mössbauer spectra of the as-prepared samples S0-S4 showed that both Sb^{3+} and Sb^{5+} ions were incorporated in the samples, as presented in figure 5. The Sb^{3+}/Sb^{5+} content ratio in the samples was determined from the relative peak areas of each species in the Mössbauer spectra as listed in table 2. It is seen that the Sb^{3+}/Sb^{5+} content ratio increases with the increase in Sb doping level up to sample S3, while for sample S4 it is smaller than for S3. Also, it was confirmed that sample S4 contained the additional phase Sb_2O_3. The ^{121}Sb-Mössbauer spectroscopy results for the annealed sample S2 (figure 6) showed that the Sb^{3+} content really decreased upon annealing. The Mössbauer spectroscopy results confirmed that the behaviour of the unit-cell parameters is determined by the Sb^{3+}/Sb^{5+} content ratio in the samples: the increase in the Sb^{3+}/Sb^{5+} content ratio causes the increase in the unit-cell parameters, and accordingly the decrease in Sb^{3+}/Sb^{5+}content ratio causes the decrease in the unit-cell parameters.

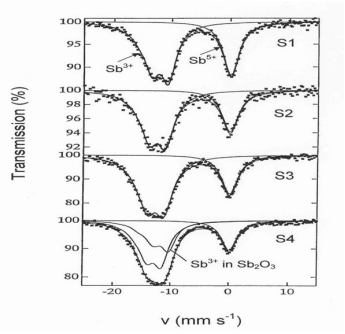

Figure 5. ^{121}Sb-Mössbauer spectra of the samples S0-S4.

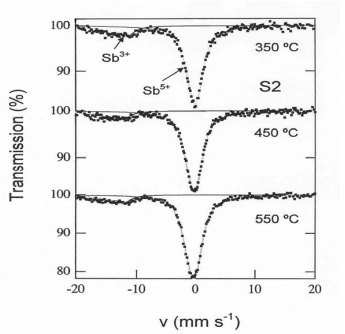

Figure 6. ^{121}Sb-Mössbauer spectra of the annealed sample S2.

Changes in full-widths at half-maximum values (FWHM) for various diffraction lines on the Sb^{3+}/Sb^{5+} content ratio were also examined. The lines 110 and 101 were chosen to calculate the FWHM ratio since their FWHM ratio strongly changed with Sb content as listed in table 2. The $FWHM_{110}/FWHM_{101}$ ratio values were determined from both the individual profile fitting and the whole-powder-pattern fitting results presented in table 1.

Table 2. Values of FWHM ratios for lines 110 and 101 and Sb^{3+}/Sb^{5+} content ratios.

ATO sample	T (°C)	$FWHM_{110}/FWHM_{101}$ by PROFIT	$FWHM_{110}/FWHM_{101}$ by WPPF	Sb^{3+} (at%)	Sb^{5+} (at%)	Sb^{3+}/Sb^{5+} content ratio
S1	20	1.31	1.27	66	34	1.9
S2	20	1.51	1.48	70	30	2.3
S3	20	1.67	1.58	74	26	2.8
S4	20	1.46	1.44	49	19	2.6
S2	350	1.09	1.07	18	82	0.2
	450	1.04	1.03	13	87	0.1
	550	1.01	1.01	10	90	0.1

The relation of the $FWHM_{110}/FWHM_{101}$ ratio and the Sb^{3+}/Sb^{5+} content ratio in the examined ATO samples is shown in figure 7. From figure 7 the following equation was derived:

$$Sb^{3+}/Sb^{5+} \text{ content ratio} = 19.9\ FWHM_{110}/FWHM_{101} - 5.8\ (FWHM_{110}/FWHM_{101})^2 - 14.1, \quad (1)$$

which is proposed for quick estimation of the Sb^{3+}/Sb^{5+} content ratio in ATO samples.

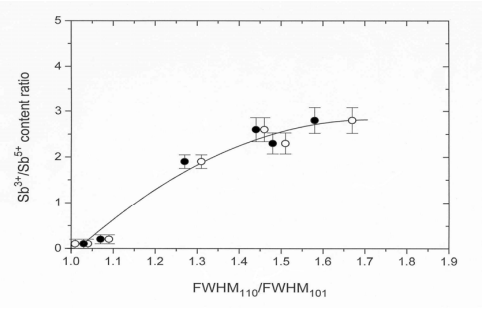

Figure 7. Relation between determined FWHM110/FWHM101 ratio and the Sb^{3+}/Sb^{5+} content ratio for the samples S0-S4. The values obtained from the PROFIT results are denoted by open circles, while those obtained from the WPPF results are denoted by solid circles.

The equation (1) suggests that the anisotropy in line broadening is present if the Sb^{3+} ions are present in the ATO structure. This is consistent with the work reported by Geurts et al. [17]. It is interesting to notice that the function (1) tends to the maximum value of Sb^{3+}/Sb^{5+} content ratio equal to 2.97 at $FWHM_{110}/FWHM_{101} = 1.71$. The method is easy and quick in comparison with spectroscopic methods. Special convenience in application of the proposed method is the fact that 110 and 101 lines are the neighbouring lines, so the XRD pattern in a narrow 2θ range (2θ=22-42 °) suffices for determination of the Sb^{3+}/Sb^{5+} content ratio.

Concluding remarks

The XRD and Mössbauer spectroscopy studies of the Sb-doped SnO_2 were performed. A correlation between $FWHM_{110}/FWHM_{101}$ ratio (obtained by XRD study) and Sb^{3+}/Sb^{5+} content ratio (obtained by ^{121}Sb-Mössbauer spectroscopy study) was found, which can be used as a basis for quick estimation of the Sb^{3+}/Sb^{5+} content ratio in ATO samples.

References

1. Orel, B., Lavrenčič-Stangar, U., Crnjak-Orel, Z., Bukovac, P. & Kosec, M., 1994*, J. Non-Cryst. Sol.*, **167**, 272.
2. Baur, W.H., 1956, *Acta Cryst. A*, **9**, 515.
3. Chopra, K.L., Major, S. & Pandya, D.K., 1983, *Thin Solid Films*, **102**, 1.
4. Crnjak-Orel, Z., Orel, B., Hodešček, M. & Kaučič, V., 1992, *J. Mater. Sci*., **27**, 313.
5. Rohatgi, A., Viverito, T.R. & Slack, L.H., 1974, *J. Am. Ceram. Soc*., **57**, 278.
6. Terrier, C., Chatelon, J.P., Roger, J.A., Berjoan, R. & Dubois, J., 1997*, J. Sol-Gel Science and Technology*, **10**, 75.
7. Tsunashima, A., Yoshimizu, H., Kodaira, K., Shimada, S. & Matsushita, T., 1986,, *J. Mat. Sci*., **21**, 273.
8. Kojima, M., Kato, H. & Gatto, M., 1993, *Philosoph. Mag. B***, 68**, 215.
9. Gržeta, B., Tkalčec, E., Goebbert, C., Takeda, M., Takahashi, M., Nomura, K. & Jakšić, M., 2002, *J. Phys. Chem. Solids*, **63**, 765.
10. Gržeta, B., Tkalčec, E., Goebbert, C., Takeda, M., Takahashi, M. & Nomura, K., 2005, in *Cristalografía. Fundamentos, Técnicas y Aplicaciones*, edited by. L. Bucio (Mexico D.F.: Sociedad Mexicana de Cristalografía A.C.), pp. 69-74.
11. Toraya, H., 1993, *J. Appl. Cryst*., **26**, 583.
12. Toraya, H., 1986, *J. Appl. Cryst.*, **19**, 440.
13. Shenoy, G.K., Friedt, J.M., Maletta, H. & Ruby, S.L., 1974, in *Mössbauer Effect Methodology*, Vol. **9**, edited by I. J. Gruverman, C.W. Seidel & D.K. Dieterly (New York: Plenum Press), p. 277.
14. Scherrer, P., 1918, *Göttinger Nachrichten*, **2**, 98.
15. Ruland, W., 1965, *Acta Cryst*., **18**, 581.
16. Popović, S., 1973, *J. Appl. Cryst*., **6**, 122.
17. Geurts, J., Rau, S., Richter, W. & Schmitte, F.J., 1984, *Thin Solid Films*, **121**, 217.